

## Studying the effect of equal channel angular extrusion on microstructure and properties of $\text{Mg}_2\text{Si}$ vehicle magnesium alloy

*F. Shen*

School of Automobile Engineering, Chongqing Three Gorges Vocational College, Wanzhou, Chongqing, China

*Received June 22, 2019*

The thermal stability of the Mg–Zn–Si magnesium alloy is investigated. The Mg–Zn–Si magnesium alloy was deformed using the ECAP process at a deformation temperature of 573 K under angular extrusion. Using the methods of optical microscopy, X-ray diffractometry, electron microscopy, and transmission electron microscopy, the characteristics of the microstructure of a deformed magnesium alloy Mg–Zn–Si are studied. The mechanical properties of the deformed alloy were tensile tested at room temperature, and creep was studied at high temperature. The results show that the  $\alpha$ -Mg matrix, the MgZn phase and the  $\text{Mg}_2\text{Si}$  phase are purified and evenly distributed with an increase in the extrusion pass number. Refining of the  $\alpha$ -Mg matrix is generated after 1-pass of extrusion. The size of  $\alpha$ -Mg decreased to 5–10  $\mu\text{m}$  after 4-pass extrusion, and the grain size was uniform. The dendrite of the  $\text{Mg}_2\text{Si}$  phase was granular in the initial position after 2-pass extrusion, and the dispersed distribution of the  $\text{Mg}_2\text{Si}$  phase was generated after 6-pass extrusion and 8-pass extrusion. The yield strength and tensile strength of the alloy were increased by 120 % after 4-pass extrusion, and the elongation of the alloy increased by 353 %. After 8-pass extrusion, the tensile strength and elongation of the alloy did not change much compared to 4-pass extrusion, but the yield strength was further increased by 19 %. As the extrusion pass number increases, the creep resistance at high temperature increases, and the constant creep rate decreases five times after 8 passes. The mechanism of grinding of the  $\text{Mg}_2\text{Si}$  phase consists in shear mechanical fragmentation.

**Keywords:** equal channel angular extrusion (ECAP),  $\text{Mg}_2\text{Si}$  Vehicle Magnesium Alloy, mechanical properties, microstructure,  $\text{Mg}_2\text{Si}$  phase.

Исследована термостойкость магниевых сплавов Mg–Zn–Si. Магниевый сплав Mg–Zn–Si был деформирован с помощью процесса ЕСАР в условиях температуры деформации 573 К и угловой экструзии. Исследованы характеристики микроструктуры деформированного магниевых сплавов Mg–Zn–Si. Механические свойства деформированного сплава испытаны на растяжение при комнатной температуре. Исследована ползучесть при высокой температуре. Результаты показывают, что матрица  $\alpha$ -Mg, фаза MgZn и фаза  $\text{Mg}_2\text{Si}$  очищаются и равномерно распределяются с увеличением проходов экструзии. Рафинирование матрицы  $\alpha$ -Mg происходит после 1 прохода экструзии. Размер  $\alpha$ -Mg уменьшился до 5–10 мкм после 4-проходной экструзии, размер зерна был однородным. Дендрит фазы  $\text{Mg}_2\text{Si}$  зернистый в исходном положении после 2-проходной экструзии; дисперсное распределение фазы  $\text{Mg}_2\text{Si}$  генерируется после 6 и 8-проходной экструзии. Предел текучести и предел прочности сплава увеличены на 120 % после 4-проходной экструзии, удлинение сплава увеличилось на 353 %. После 8-проходной экструзии прочность на растяжение и относительное удлинение сплава мало изменились по сравнению с 4-проходной экструзией, но предел текучести дополнительно увеличивается на 19 %. С увеличением прохода экструзии сопротивление ползучести при высокой температуре увеличивается, а постоянная скорость ползучести уменьшается в пять раз после 8 проходов. Механизм измельчения фазы  $\text{Mg}_2\text{Si}$  заключается в механической фрагментации при сдвиге.

### Дослідження впливу кутової екструзії на мікроструктуру і властивості магнієвого сплаву $Mg_2Si$ . F. Shen.

Досліджено термостійкість магнієвого сплаву  $Mg-Zn-Si$ . Магнієвий сплав  $Mg-Zn-Si$  деформовано за допомогою процесу ЕСАР в умовах температури деформації 573 К і кутової екструзії. Методами оптичної мікроскопії, рентгенівської дифрактометрії, електронної мікроскопії, що просвічує, електронної мікроскопії досліджено характеристики мікроструктури деформованого магнієвого сплаву  $Mg-Zn-Si$ . Механічні властивості деформованого сплаву випробувано на розтяг при кімнатній температурі, досліджувалася повзучість при високій температурі. Результати показують, що матриця  $\alpha-Mg$ , фаза  $MgZn$  і фаза  $Mg_2Si$  очищаються і рівномірно розподіляються зі збільшенням проходу екструзії. Рафінування деякої матриці  $\alpha-Mg$  генерується після 1 проходу екструзії. Розмір  $\alpha-Mg$  зменшився до 5–10 мкм після 4-прохідної екструзії, і розмір зерна був однорідним. Дендрит фази  $Mg_2Si$  зернистий в початковому положенні після 2-прохідної екструзії, і дисперсний розподіл фази  $Mg_2Si$  генерується після 6-прохідної і 8-прохідної екструзії. Межа плинності і межа міцності сплаву збільшені на 120 % після 4-прохідної екструзії, а подовження сплаву збільшилося на 353 %. Після 8-прохідної екструзії міцність на розтягнення і відносне подовження сплаву мало змінилися у порівнянні з 4-прохідною екструзією, але межу плинності додатково збільшено на 19 %. Зі збільшенням проходу екструзії опір повзучості при високій температурі збільшується, а постійна швидкість повзучості зменшується у п'ять разів після 8 проходів. Механізм подрібнення фази  $Mg_2Si$  полягає у механічній фрагментації при зсуві.

## 1. Introduction

Magnesium and Vehicle Magnesium Alloys are one of the most promising lightweight materials with the advantages of low density, high specific strength and specific stiffness, excellent shock absorption, excellent damping, excellent electromagnetic shielding and environmental friendliness [1]. Up to now, high-performance Vehicle Magnesium Alloys have been widely used in aerospace industry, motor vehicles, electronic information materials and other fields. However, the application of Vehicle Magnesium Alloys is greatly restricted due to their own deficiencies, such as low strength, poor plastic deformation ability, poor high temperature performance, poor corrosion resistance and poor formability, etc. Among them, improving the high temperature properties of Vehicle Magnesium Alloys becomes an important research direction [2]. At the same time, the high cost of high-performance Vehicle Magnesium Alloys limits the their further promotion and application, so the development of a low cost and excellent properties of Vehicle Magnesium Alloys is a hot topic in the field of materials [3].

Therefore, on the basis of previous studies, an ECAP deformation mechanism for refinement of  $Mg_2Si$  phase in  $Mg-Zn-Si$  alloy, and the mechanism of influence of relative high temperature on creep properties of  $Mg_2Si$  were studied in this paper.

Equal channel angular extrusion (ECAP) is a material processing technology invented

by a former Soviet scientist Segal in the 1970s. It is one of the effective methods to obtain sub-micron ultra-fine grain materials and nano-materials [4]. Since then, the ECAP technology has been used to deform aluminum alloy, titanium alloy, copper alloy and Vehicle Magnesium Alloy; the grain refinement of the materials has been successfully realized and the properties of the materials have been improved. The microstructure of pure magnesium after one pass of the ECAP deformation was studied by Majdi et al. It was found that the grain size of the material after the deformation was significantly finer than that of the coarse grain before the deformation [5]. In order to study the effect of the ECAP deformation passes on the microstructure and properties of the materials at room temperature, Ghandvar et al. realized 8 pass deformations with pure aluminum rods as test materials [6]. The results show that there is no difference in grain size between cross-section and longitudinal section after the 8-pass deformation, and the yield strength of the material after the 4-pass deformation reaches the maximum value [7]. In addition, the ECAP allows one to obtain the microstructure of ultra-fine grained materials, and to carry out the multi-pass extrusion deformation without changing the shape of the materials. At the same time, it can also heal the microstructure defects such as micropores and improve the compactness of the materials, etc. [8].

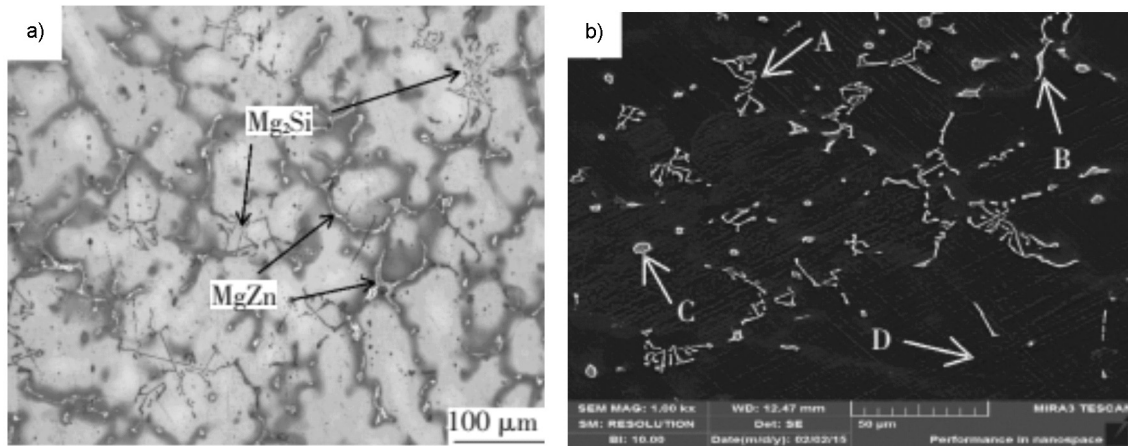


Fig. 1. Microstructure of experimental cast alloy.

## 2. Experimental

### 2.1 Studying materials and reagents

The Vehicle Magnesium Alloy used in this paper is a self-made alloy, which is melted in a SG-5-12 well crucible resistance furnace. The actual composition (mass fraction / %) of the alloy is 4.9 Zn, 1.0 Si, and the remainder is Mg. The ingot was cut into extrusion specimen of 55 mm×10 mm×100 mm. The specimen was extruded at 573 K by C path 1-8 pass extrusion, by using Equal Channel Angular Extrusion die with an internal angle of 90° and a diplomatic angle of 20°. The metallographic sample was intercepted from the middle of the extruded sample. The corrosion agents of picric acid (5 g picric acid + 78 mL alcohol + 7 mL distilled water + 10 mL glacial acetic acid) were prepared. The microstructure was observed by CMM-20 optical microscope. The tensile test sample was cut along the extrusion direction, and the dimension at the standard distance was 40 mm×4.5 mm×2 mm. The tensile test was carried out with the DNS100 electronic universal tester, and the tensile rate was 0.5 mm/min [9]. A KY2-2000 X-ray diffractometer (XRD) was used to analyze the phase composition, a JSM6700-F scanning electron microscope was used to observe the fracture morphology, a JEM2000EX type transmission electron microscope was used to observe the microstructure and dislocation configuration in the micro-region. The YHD displacement gauge and YE2539 high-speed static strain gauge were used to test creep resistance at high temperature [10].

### 2.2 Research equipment

The main equipment used for melting alloy: the melting furnace adopts SXZ-5-2 type well crucible resistance furnace, and

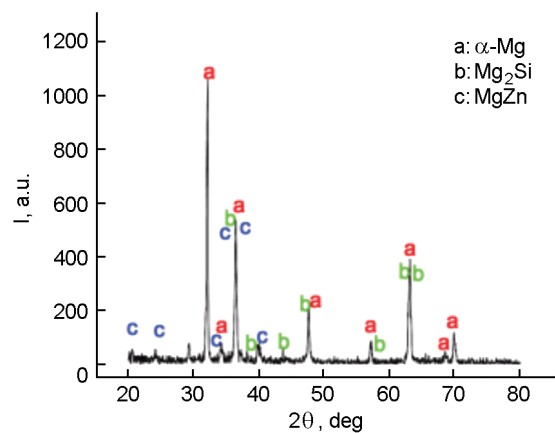


Fig. 2. Phase analysis spectrum of as-cast alloy.

its rated power is  $P = 7$  kW, rated temperature  $T = 1473$  K [11]. The type of temperature control box is the KSW-3-11 temperature controller, and the type of drying equipment is 101A-2 type blast oven. Before melting, the raw materials and the ground covering and refining agents (as shown in Table 2-2) are put into the drying oven and adjusted to 423 K to dry the raw materials. During the melting process, a mixture of carbon dioxide (CO<sub>2</sub>) and sulphur hexafluoride (SF<sub>6</sub>) is used as a protective gas, and the two gases are first mixed uni-

Table 1. Energy spectrum analysis of phase components in Fig. 1(b), (at. %)

Position	Mg	Zn	Si
A	67.7	0.2	32.1
B	49.2	50.8	0
C	63.1	36.9	0
D	96.4	1.3	2.2

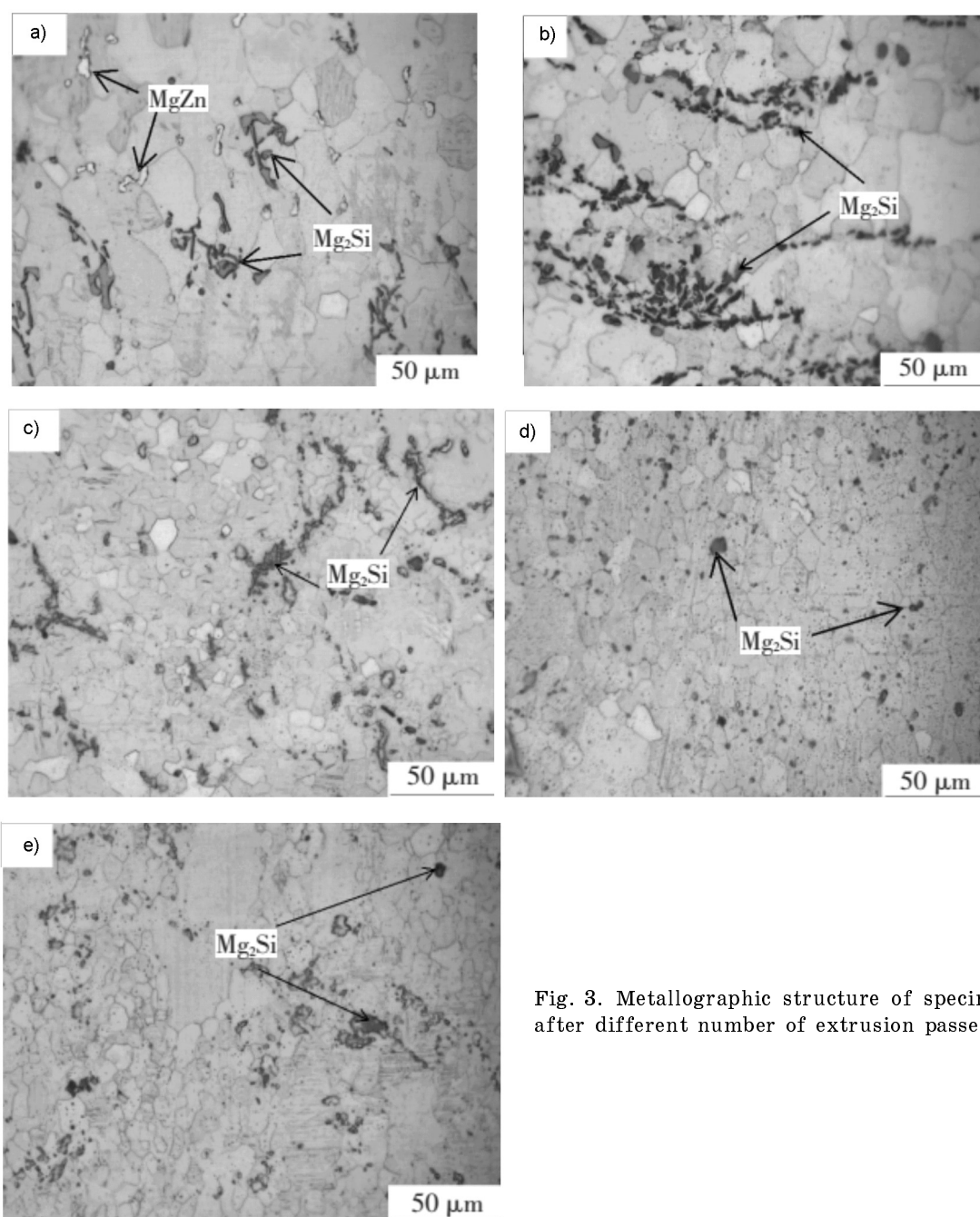


Fig. 3. Metallographic structure of specimen after different number of extrusion passes.

formly ( $\text{VCO}_2/\text{VSF}_6 = 40/1$ ) in the mixing cylinder. The mixture is then put into the melting furnace to protect the molten alloy from oxidation [12]. After melting, the molten liquid is poured into the cylindrical die (shown in Fig. 2, 3). The bar was cut into samples of  $12.3 \text{ mm} \times 12.3 \text{ mm} \times 55 \text{ mm}$  by a DK7728 EDM numerical control wire cutting machine. Before the extrusion deformation test, the samples to be extruded were grinded step by step with 400, 600, 1200, 250 # sandpaper in order to remove the oxide layer on the sample surface, and then the

equal channel angular extrusion die was used for ECAP deformation at 573 K. The middle part of the deformed sample was inter-

Table 2. Mechanical properties of as-cast and 4 and 8-pass extruded alloy at room temperature

Passes	$\sigma_s$ , MPa	$\sigma_b$ , MPa	$\delta$ , %
as-cast	56	128	3.2
4 passes	123	282	14.5
8 passes	146	283	14.2

cepted and polished and corroded (see Table 2–3 for the composition of the corrosion inhibitor). The microstructure and phase composition were observed by the DM2700MRL optical microscope (OM), JSM6700-F scanning electron microscope and (SEM), KY2-2000 X-ray diffractometer, respectively.

### 3. Results and discussion

The experimental results are shown in Fig. 1, Fig. 2 and Table 1. Table 1 shows the energy spectrum results of the phase in Fig. 1(b). The MgZn phase is distributed discontinuously on the grain boundary and  $\alpha$ -Mg dendrite boundary. The  $\text{Mg}_2\text{Si}$  phase is distributed in the shape of Chinese characters within and near the grain boundary. The  $\alpha$ -Mg grain size of the matrix is 100 ~ 200  $\mu\text{m}$ , and the primary dendrite length of the  $\text{Mg}_2\text{Si}$  phase is up to 80  $\mu\text{m}$ . Fig. 3 shows the microstructure of ECAP deformation after 1, 2, 4, 6, 8 passes. As can be seen from Fig. 3(a), after one pass of deformation, the  $\alpha$ -Mg matrix is refined to 20–50  $\mu\text{m}$ , and the MgZn phase is refined into fine particles. After 2 passes, the  $\alpha$ -Mg matrix was further refined, and all the dendrites of  $\text{Mg}_2\text{Si}$  phase were broken into granular shape. The particles of  $\text{Mg}_2\text{Si}$  phase were concentrated in the original position, and with the increase of the extrusion pass number, the particles of  $\text{Mg}_2\text{Si}$  phase tended to dispersive distribution. As shown in Fig. 3(c), (d), (e), the MgZn phase is further refined and tends to be uniformly distributed. After 4 passes, the  $\alpha$ -Mg matrix is refined to 5–10  $\mu\text{m}$ , and the grain size tends to be uniform; the particles of the  $\text{Mg}_2\text{Si}$  phase are further fragmented, and some of them leave the original position and tend to dispersive distribution. After 6 and 8 passes of the extrusion, most of  $\alpha$ -Mg grains of the matrix are about 5  $\mu\text{m}$ . A few of the grains grow up abnormally, and the  $\text{Mg}_2\text{Si}$  phase particles become very fine and distributed in a dispersive form.

The mechanism of  $\alpha$ -Mg refinement by the ECAP deformation is continuous dynamic recrystallization, which has been reported by many authors. A part of grain refinement after one pass is due to the discontinuous, pure shear deformation of the ECAP deformation. Due to non-uniform deformation, shear bands appear in some grains (as shown in Fig. 4); high-density dislocation entanglement in the shear bands provides en-

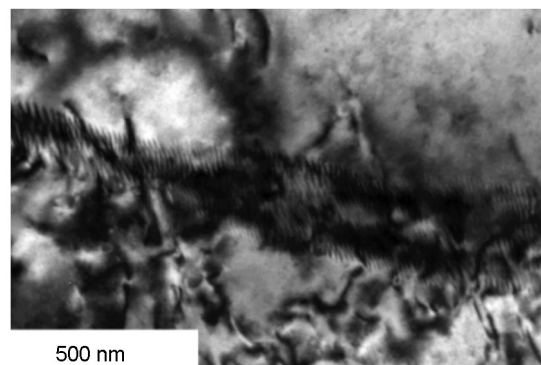


Fig. 4. Shear band structure of experimental alloy formed by ECAP.

ergy conditions for dynamic recrystallization resulting in uneven grain size.

Fig. 5 shows the  $\text{Mg}_2\text{Si}$  phase morphology in the ECAP deformation; Fig. 5(a) is a TEM photograph of the experimental alloy, Fig. 5(b) is an EDS spectrum of the e-point in Fig. 5(a), and the conjugation phase analysis (Fig. 2) shows that the particles in Fig. 5 (a) are the result of  $\text{Mg}_2\text{Si}$  brittleness, since this phase is prone to brittle fracture when subjected to stress. The shear-slip band formed in the  $\alpha$ -Mg matrix is hindered by the  $\text{Mg}_2\text{Si}$  phase in the process of expansion, and dislocations accumulate in  $\text{Mg}_2\text{Si}$  to produce stress concentration. When the dislocations in the plug reach a sufficient number, the total stress generated is sufficient to cause cracks in the  $\text{Mg}_2\text{Si}$  phase, resulting in shear separation. As shown in Fig. 5(a), (c), the  $\text{Mg}_2\text{Si}$  phase broken by mechanical shear gradually tends to disperse with the increase of the extrusion pass number; as shown in Fig. 5(d), like the  $\alpha$ -Mg matrix, the  $\text{Mg}_2\text{Si}$  phase particles cannot be fine infinitely. When the critical stress required for brittle fracture of fine particles is greater than the applied stress, the  $\text{Mg}_2\text{Si}$  phase particles will not fracture but remain within a certain size range, as shown in Fig. 5.

The mechanical properties of the experimental alloys at room temperature are shown in Table 2 and Fig. 6. The as-cast alloy has yield strength of 56 MPa, tensile strength of 128 MPa and elongation of 3.2 % because of the strong action of the  $\text{Mg}_2\text{Si}$  phase on the splitting of the matrix and easy producing stress concentration. After the 4-pass extrusion, the  $\alpha$ -Mg matrix is refined, the  $\text{Mg}_2\text{Si}$  and MgZn phases are not only refined but also tend to dispersive distribution, and mechanical properties are greatly improved. After the 8-pass ex-

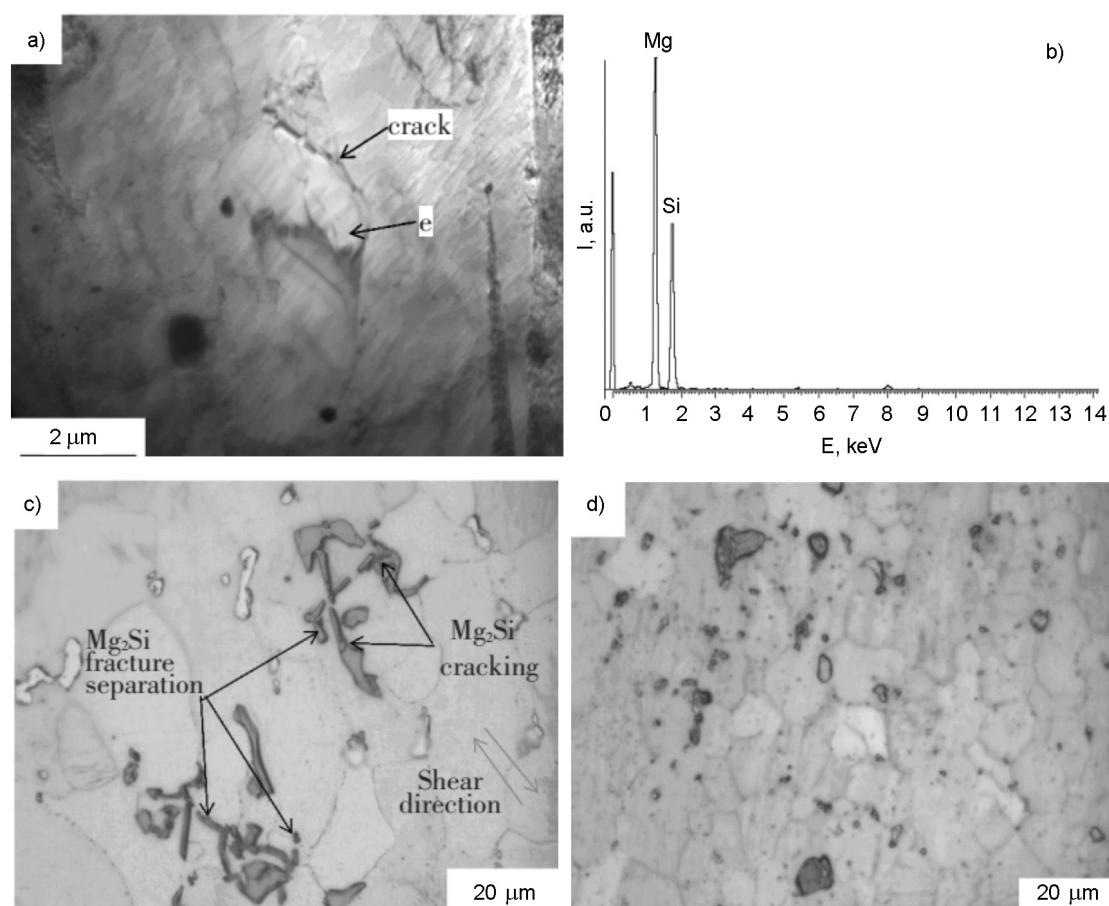


Fig. 5. Morphology change of Mg<sub>2</sub>Si phase after deformation by ECAP.

trusion, the  $\alpha$ -Mg matrix does not change much compared with the result of 4 passes. However, the distributions of the Mg<sub>2</sub>Si and MgZn phases are more uniform; the Mg<sub>2</sub>Si phase particles become obtuse, the MgZn phase particles become round and the second phase has better strengthening effect, so the yield strength is further improved. As can also be seen from Fig. 6, after 4 and 8 passes of deformation the stress-strain curve shows a serrated shape which may be due to the sawtooth yield phenomenon caused by dynamic strain aging; this result needs to be further studied.

Fig. 7 shows the tensile fracture morphology of the experimental alloy at room temperature. The tensile fracture of the as-cast alloy has no obvious macro-plastic deformation, and the fracture is relatively homogeneous and perpendicular to the tensile axis. As shown in Fig. 7(a), there are obvious fracture planes, cleavage steps and tearing edges on the fracture surface, and there are more secondary cracks on the fracture surface. A large number of the fracture

planes in Fig. 7(a) are at the interface between  $\alpha$ -Mg and flake Mg<sub>2</sub>Si phases. When the dislocation moves under stress, it encounters the Mg<sub>2</sub>Si phase and plugs, resulting in a large stress concentration at the front of the plug. Because of the low interfacial bonding strength between the Mg<sub>2</sub>Si phase and  $\alpha$ -Mg matrix, the formation and propagation of cracks is beneficial, and the pinning dislocations can move, resulting in plastic deformation and decrease of yield strength. With the increase of load, the dislocations encounter cracks, and the dislocations disappear while cracks grow rapidly. These cracks easily propagate along the interface of Mg<sub>2</sub>Si/ $\alpha$ -Mg phase until fracture, which leads to the low elongation and tensile strength of the alloy.

After 4 passes of extrusion, plastic deformation can be observed near the tensile fracture surface. The whole fracture plane and the tensile axis are at 45° angle. The micro-characteristics of the fracture surface are shown in Fig. 7(b); the second phase of Mg<sub>2</sub>Si is fine-grained. Therefore, there is no

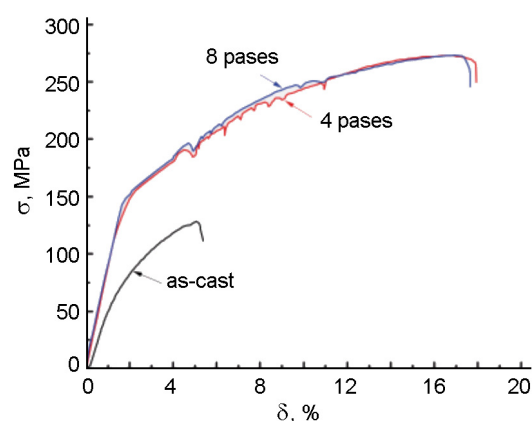


Fig. 6. As-cast and ECAP extruded 4 and 8-pass stress-strain curves.

fracture plane on the fracture surface (the  $\alpha$ -Mg and flake  $Mg_2Si$  phase interface), the  $\alpha$ -Mg matrix and the MgZn phase on the grain boundary are refined, and there are no obvious cleavage steps on the fracture surface, showing a large number of fine dimples. The granular second phase exists at the bottom of some dimples. It is further proved that the fine grain strengthening and the second phase strengthening are the reasons for the improvement of mechanical properties of the ECAP deformed experimental alloy. Some quasi-cleavage fracture morphology on the fracture surface is observed because a small number of  $\alpha$ -Mg matrix grains are still coarse.

Under conditions of creep at temperature 523 K and stress 60 MPa, as-cast, 4-pass and 8-pass creep tests were carried out respectively. The experimental results are shown in Fig. 8 and Table 3.

It is easy to produce stress concentration around Chinese character  $Mg_2Si$  phase in

cast state. When the stress concentration reaches a certain extent, a wedge crack is easily formed. These cracks lead to relaxation of the stress concentration, resulting in continuous generation and slip of dislocations. Then the stress concentration is generated again. Because the crack easily propagates along the interface between the  $Mg_2Si$  phase and matrix, the crack propagation speed is accelerated and the crack propagation is rapidly entered the instability growth stage. Therefore, the creep curve of the as-cast alloy is directly changed from stage 1 to stage 3. The fracture takes place in a short period of time. After equal channel extrusion, the creep resistance of the Mg-Zn-Si Vehicle Magnesium Alloy is greatly improved, which is related to its microstructure, especially the size and distribution trend of  $Mg_2Si$  reinforcing particles in the second phase; that is, under the experimental temperature and stress, the steady-state creep rate decreases with the refinement and dispersive distribution of the  $Mg_2Si$  reinforcing phase in the Mg-Zn-Si alloy. Under the action of constant temperature and constant stress, the  $Mg_2Si$  phase particles can effectively pin the dislocations and improve the creep resistance. Generally speaking, the creep resistance at high temperature should decrease with grain refinement, but the result of this experiment is opposite.

With the increase of the extrusion pass number, both grain refinement and creep resistance at high temperature are improved. The reason is that the deformation of the ECAP changes the grain boundary structure while the grain is refined, so that a large number of dislocations are accumulated at the grain boundary (as shown in Fig. 9), the dislocations are prevented from further slipping, the dislocations are entangled, sliding by the

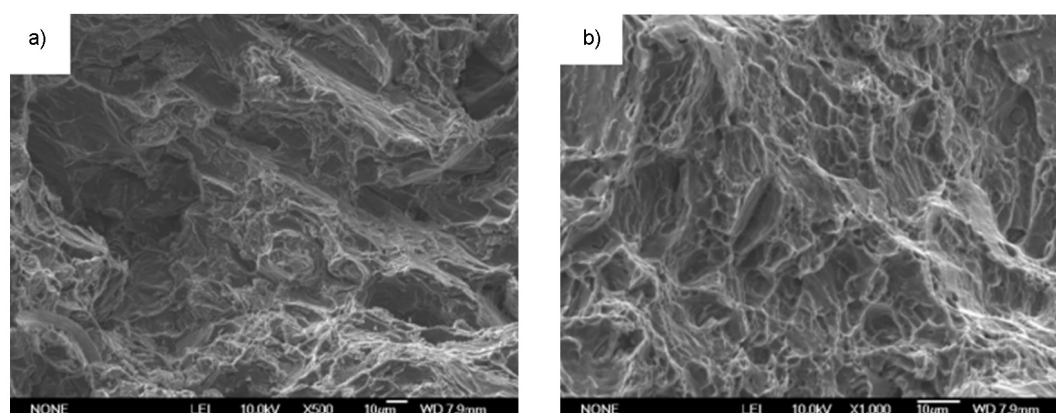


Fig. 7. Sample fracture morphology at room temperature

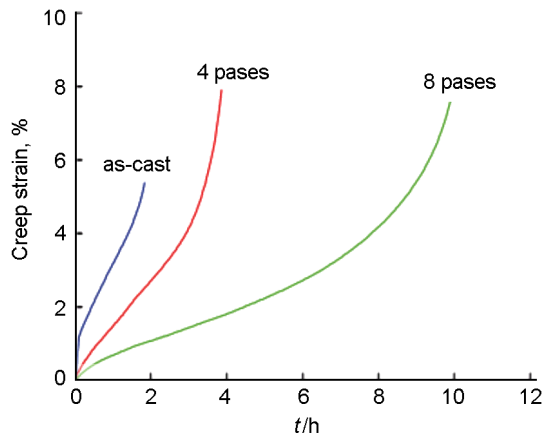


Fig. 8. Creep curve of specimen at 523 K, 60 MPa.

Table 3. Creep properties of specimens with different extrusion passes

Passes	T, K	$\sigma$ , MPa	$\varepsilon$ , %	Creep rate $\dot{\varepsilon}$	t, h
0p	523	60	5.40	2.16	1.83
4p			7.99	1.31	3.87
8p			7.68	0.39	10.09

grain boundary is difficult at high temperature, and the grain boundaries play a reinforcing role in the high-temperature creep. At the same time, the dispersive distribution of the second phase ( $\text{Mg}_2\text{Si}$ ,  $\text{MgZn}$  particles) in the crystal and grain boundary and pinning the dislocations can improve the creep resistance at high temperature.

#### 4. Conclusions

Both the matrix microstructure of  $\text{Mg-Zn-Si}$  alloy and the Chinese-shaped  $\text{Mg}_2\text{Si}$  phase were refined by ECAP deformation. The mechanism of  $\text{Mg}_2\text{Si}$  phase refinement is mechanical breaking due to shear. With the increase of the extrusion pass number, the microstructure became more uniform.

The interface of Chinese character of the  $\text{Mg}_2\text{Si}$  phase and  $\alpha\text{-Mg}$  phase in the as-cast  $\text{Mg-Zn-Si}$  alloy becomes a crack source and a crack propagation channel, resulting in low mechanical properties. After ECAP deformation, the magnesium matrix is refined. Especially, the second  $\text{Mg}_2\text{Si}$  phase is obviously refined and uniformly distributed in the matrix; thus, the  $\text{Mg}_2\text{Si}$  phase re-

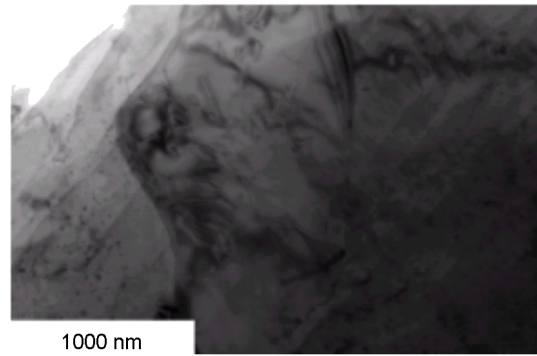


Fig. 9. Grain boundary structure of specimen after ECAP deformation.

duces the splitting effect of the matrix and acts as a pinning dislocation, which greatly improves the mechanical properties of the alloy at room temperature.

The ECAP deformation not only refines the microstructure but also changes the grain boundary structure. The pinning effect of dislocations and the second relative grain boundary is greater than the decrease of the grain size, which results in the decrease of creep property and thus the creep resistance at high temperature is improved.

#### References

1. W.Wang, H.Wang, Y.Liu et al., *J. Mater. Res.*, **32**, 615 (2017).
2. L.I.Lei-Liang, T.J.Chen, S.Q.Zhang, S.Y.Cai, *J. Plasticity Eng.*, **3**, 164 (2016).
3. H.Wang, L.Feng, C.Lei et al., *Mater. Sci. Eng. A*, **657**, 331 (2016).
4. H.Zhang, T.L.Wang, W.Y.Liu et al., *J. Plasticity Eng.*, **24**, 36 and 46 (2017).
5. H.Majdi, A.Razaghian, M.Emamy, N.Motalebi, *Adv. Mater. Process. Techn.*, **3**, 164 (2017).
6. H.Ghandvar, M.H.Idris, N.Ahmad, *J. Alloys Compounds*, **751**, S0925838818314324 (2018).
7. D.Zhang, X.Hao, D.Fang, Y.Chai, *Rare Metal Mater. Eng.*, **45**, 2208 (2016).
8. Y.Wang, Y.Zhang, G.Wei, *Intern. J. Modern Phys. B*, 31 (2017).
9. L.Zheng, H.Nie, L.Wei et al., *J. Magnesium & Alloys*, **4**, 115 (2016).
10. H.Zengin, Y.Turen, *Mater. Chem. Phys.*, 214 (2018).
11. X.Xu, W.Jiang, P.Deng et al., *Rare Metal Mater. Eng.*, (2017).
12. K.Horvath, D.Drozdenco, G.Garces et al., *Acta Phys. Polonica Ser. A*, **134**, 815 (2018).